Nanoscale

Accepted Manuscript

This article can be cited before page numbers have been issued, to do this please use: L. Zou, R. Li, M. Zhang, Y. Luo, N. Zhou, J. Wang and L. Ling, *Nanoscale*, 2017, DOI: 10.1039/C6NR09089C.

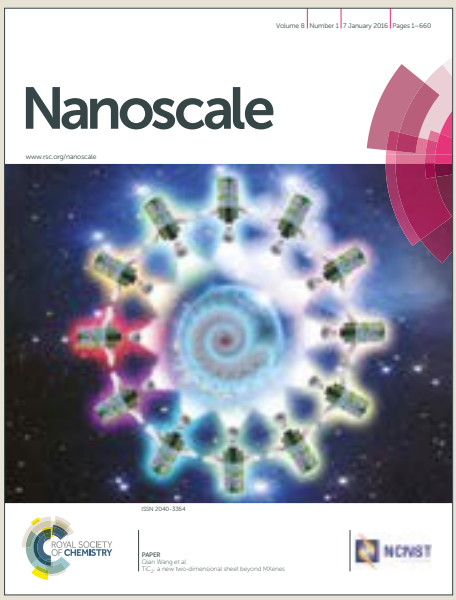

ROYAL SOCIETY OF CHEMISTRY

rsc.li/nanoscale

View Article Online
DOI: 10.1039/C6NR09089C

Nanoscale

PAPER

Colorimetric sensing platform based upon recognizing hybridization chain reaction product with oligonucleotide modified gold nanoparticles through triplex formation

Received 00th January 20xx,
Accepted 00th January 20xx

DOI: 10.1039/x0xx00000x

www.rsc.org/

Li Zou,‡ Ruimin Li,‡ Manjun Zhang, Yanwei Luo, Nian Zhou, Jing Wang and Liansheng Ling*

A novel colorimetric sensing strategy for biomolecules assay has been developed, which integrates the signal amplification of hybridization chain reaction (HCR) with the assembly of gold nanoparticles (AuNPs) through triplex formation. In the presence of targets, the HCR process can be triggered, the HCR products are specifically recognized by triplex-forming oligonucleotide (TFO) functionalized AuNPs, accompanying the aggregation of AuNPs and a dramatic absorbance change at 522 nm. In addition, the DNA hairpin probes can form rigid triplex structures with TFO-functionalized AuNPs in the absence of targets, resulting in a negligible background signal. By taking advantage of this new biosensor platform, a broad range of targets, involving nucleic acids, small molecules and proteins, have been successfully determinated with high sensitivity and selectivity, which may hold great potential for practical application.

Introduction

Developing effective methods with high sensitivity and low background noise to determinate biomarkers is of great significance in the field of disease diagnosis, food security and environmental protection.[1-3] Many current in-vitro amplification techniques, including polymerase chain reaction (PCR), rolling-circle amplification (RCA), strand-displacement amplification (SDA), helicase-dependent amplification (HAD), hybridization chain reaction (HCR), have been designed by employing interdisciplinary strategies involving chemistry, biology, and materials science, and achieved high selectivity and sensitivity.[4] Among them, HCR, first put forward by Dirks and Pierce in 2004, has been extensively employed in bioanalysis because of its enzyme-free feature, autonomous protocol and efficient isothermal amplification capability.[5-7] Although the HCR nature empowers amplified sensing platforms to carry out at room temperature without the use of thermal cycler and enzymes, it also suffers from inevitable challenges that is limited sensitivity, poor ability in practical applications and high background noise. About these problems, many improved strategies have been proposed.[8-10] Recently, Fan et al. combined the tetrahedral DNA nanostructure probes which were obtained by self-assembly of four single stranded DNA, and HCR amplification to establish an electrochemical biosensor, greatly improving sensitivity and lowering background signals.[11] However, in accordance with selectivity, specificity, accuracy and automation, advanced analytical methods based on new technologies are still in demand.

Triplex nucleic acid formation, first discovered by Davies and Rich in 1956, occurs when a triplex-forming oligonucleotide (TFO) binds to a specific region of double-stranded DNA (dsDNA). The TFO has two types, oligopyrimidine and oligopurine, which can recognize homopyrimidine·homopurine duplex DNA via Hoogsteen (or reverse-Hoogsteen) hydrogen bonds.[12, 13] As a powerful tool, the triple helix interaction plays an important role in regulating gene expression, constructing molecular switches for biosensing platforms, sequence-specific recognition of the natural state of dsDNA and manipulating DNA nanostructures.[14-20] For example, Wang et al. reported an integrated sensing platform for ultrasensitive and selective detection of DNA by using graphene-mesoporous silica-gold NP hybrids as an enhanced element, strand-displacement DNA polymerization and parallel-motif DNA triplex system as dual amplifications.[21] Although many impressive advances have been made in the design of TFOs, triplex technology is still in immaturity. Therefore, development of novel amplification techniques based on triplex DNA offers the prospect of ideal assays which have the ability to efficiently amplify biomarkers and produce a highly sensitive signal with low background.

Au nanoparticle probes are ideal colorimetric signal reporters due to their remarkably high extinction coefficient and strongly distance-dependent photonic properties. Unmodified AuNPs was employed in HCR-based assays based upon their different physical adsorption ability between ssDNA and dsDNA.[22] Positive charged AuNPs was used as probe based upon the huge negative charge of HCR product.[23] Herein, we propose a triplex DNA-assisted HCR strategy for highly sensitive and selective detection of a broad

School of Chemistry, Sun Yat-Sen University, Guangzhou 510275, P. R. China. E-mail: cesllsh@mail.sysu.edu.cn.

‡ Li Zou and Ruimin Li contributed equally to this work.

Electronic Supplementary Information (ESI) available: [Experimental details and additional figures]. See DOI: 10.1039/x0xx00000x

View Article Online
DOI: 10.1039/C6NR09089C

range of targets, including nucleic acid sequences, proteins and small molecules, using the absorbance change at 522 nm due to the aggregation of gold nanoparticles. Triplex DNA is employed as a pivot to integrate the HCR with the gold nanoparticles, which is different from a triple helix molecular switch regulating the process of HCR reported by Yang et al. previously.[24] The present work concludes triplex-forming oligonucleotide functionalized gold nanoparticles (AuNPs-TFO), three DNA hairpin probes (HP, H1 and H2). In the absence of targets, the hairpin DNA probes H1 and H2 can form a rigid triplex structure with AuNPs-TFO via Hoogsteen base pairing, which makes the system stable and results in a relatively low background signal. In the presence of targets, the HCR process can be triggered. The obtained long-nicked dsDNA products are easily recognized by AuNPs-TFO via triplex formation, resulting in the aggregation of gold nanoparticles and a dramatic absorbance change at 522 nm. This approach not only has universality for the sensitive and selective colorimetric detection of biomarkers, but also provides great potential to be applied in practical samples.

Results and discussion

Principle for colorimetric target assay

The principle of the colorimetric sensing strategy based on the HCR amplification and the assembly of gold nanoparticles through triplex formation is illustrated in Scheme 1. In the absence of targets, the HCR process cannot be triggered, thus three DNA hairpin probes (HP, H1 and H2) can coexist stably in solution. The sensing system can be stabilized through forming rigid triplex structures by AuNPs-TFO, H1 and H2, resulting in no obvious change at 522 nm and a negligible background signal. While in the presence of targets, the aptamer sequences in HP recognize targets to form the target-HP complex, the exposed fragment originally caged in HP pairs with the sticky end of H1, which undergoes a toehold-mediated strand displacement reaction (TMSDR) to open the hairpin. The newly exposed domain of H1 nucleates at the sticky end of H2 to open the hairpin and expose a new fragment on H2, whose sequence is identical to that of the fragment in HP, which can hybridize with the sticky end of another H1. In this manner, each copy of the target can initiate the chain-like assembly of H1 and H2 to form a long-nicked double-helix. After the addition of AuNPs-TFO, the triplex DNA forms between HCR products and TFO, results in the formation of cross-linked network of AuNPs and a dramatic absorbance change at 522 nm, which can be estimated by UV-vis spectroscopy.

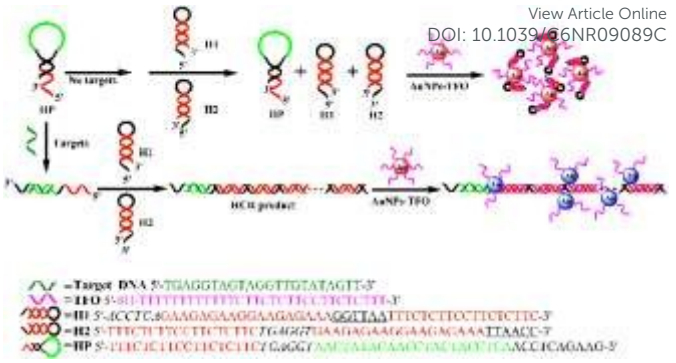

Scheme 1 Schematic illustration of the design strategy for the colorimetric detection of target based on the hybridization chain reaction amplification and the assembly of gold nanoparticles. Three DNA hairpin probes (HP, H1 and H2) were ingeniously designed to construct the sensing system for cascaded signal amplification (the DNA sequences were listed in Table S1, ESI†). DNA-functionalized gold nanoparticles were used as AuNPs-TFO to form a triplex structure via Hoogsteen base pairing with the dsDNA product of HCR.

Feasibility study of colorimetric target assay

To demonstrate the viability of this strategy, the proof-of-principle experiments were carried out for target DNA detection. As shown in Fig. 1A, in the absence of target DNA, a surface plasmon resonance absorption peak at 522 nm for TFO-functionalized AuNPs dispersion was observed, and the color of the solution appeared red (inset in Fig. 1A), indicating that the hairpin probes were stable and no assembly of gold nanoparticles occurred without target DNA. On the other hand, in the presence of 5.0 nM target DNA, the absorbance band at 522 nm decreased significantly. Correspondingly, the color of the solution changed from red to blue due to a bathochromic shift of the nanoparticle plasmon resonance (inset in Fig. 1A). The target DNA induced aggregation of TFO-functionalized AuNPs was confirmed by dynamic light scattering (DLS) results and transmission electron microscopy (TEM) images. As shown in Fig. 1B, the average hydrodynamic diameter of the dispersed TFO-functionalized AuNPs was around 38.5 nm. The morphology of the particles was characterized by TEM (Fig. 1D), and it showed the TFO-functionalized AuNPs were well dispersed with a narrow size in the range of 13-20 nm. The hydrodynamic diameter of TFO-functionalized AuNPs measured by DLS was slightly larger than the actual size of the particles measured by TEM. This is not unexpected, because DLS is a bulk analysis method and gives an average based on a number distribution which is derived from the intensity distribution of scattered light. It has been reported previously in the literature, as a light scattering/Brownian motion based technique, DLS is known to be biased toward detecting larger particles within a suspension.[25, 26] As a result, the hydrodynamic diameter measured from the random thermodynamic motion of the particles (Brownian motion) is greater than the actual size of the particles.[27] Upon addition of 5.0 nM target DNA, the average hydrodynamic diameter of TFO-functionalized AuNPs increased to 769.0 nm (Fig. 1C), and the large DNA-linked three-dimensional aggregates was clearly observed from the TEM image (Fig. 1E).

In addition, as can be seen from electrophoresis gel images, in the HCR system (Fig. S1A), new smears appeared when the target mixed with three DNA hairpin probes, suggesting HCR had taken place. In the triplex system (Fig. S1B), new bands appeared when dsDNA molecules interacted with TFO, indicating that triplex formation had occurred. Meanwhile, as shown in the circular dichroism spectroscopy (Fig. S2), a negative peak at 210 nm appeared with the addition of targets, which was the marker for triplex DNA.[28] Furthermore, to verify the assumption that AuNPs-TFO can specifically recognized the dsDNA products of HCR, lambda DNA was added into the sensing system. As shown in Fig. S3, lambda DNA could not be recognized by AuNPs-TFO, the aggregation of AuNPs did not appear. These results indicated that triplex DNA was formed between HCR products and TFO in the presence of targets. Target DNA could trigger a cascade of hairpin hybridization events to yield numerous long nicked dsDNA molecules, which interacted with TFO-functionalized AuNPs to form a cross-linked network of gold nanoparticles. Therefore, the strategy that employed triplex DNA formation for the assembly of AuNPs to induce the absorbance change at 522 nm as the signals had certain feasibility.

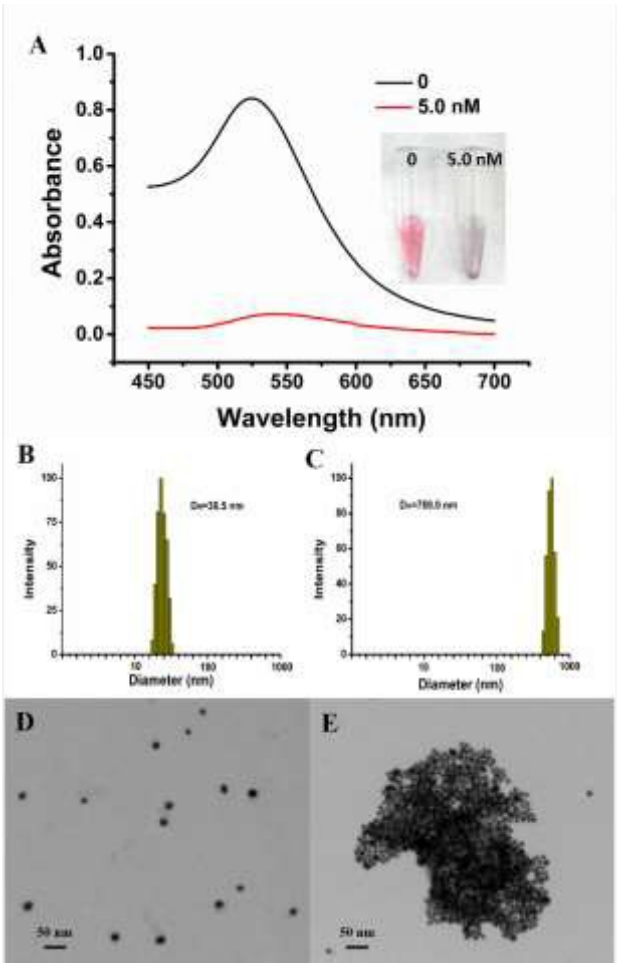

Fig. 1 (A) UV-vis absorption spectra of the colorimetric sensing system in the absence and presence of target DNA (5.0 nM). Inset: photographs of target-induced color change of the DNA-functionalized AuNPs dispersion. (B) DLS measured hydrodynamic size distribution of the dispersed DNA-functionalized AuNPs. (C) DLS measured hydrodynamic size distribution of the DNA-functionalized AuNPs assembly in the presence of 5.0 nM target DNA. (D) TEM image of the dispersed DNA-functionalized AuNPs. (E) TEM image of a microscopic DNA-functionalized AuNPs assembly in the presence of 5.0 nM target DNA. Scale bar: 50 nm.

Optimization of assay conditions

The pH value plays an important role in the sensing process. As shown in Fig. 2A, the aggregation degree (AD = $\Delta A/A_0$,[29] A_0 is the initial absorption value of the system at 522 nm, ΔA is the value of absorbance change at 522 nm) of the system containing 5.0 nM target DNA slightly changed at acidic pH, while the ΔAD of the sensing system would then increase obviously with the pH ranging from 5.0 to 6.5. Meanwhile, the value of AD sharply decreased as expected when pH value increased from 6.5 to 7.0, due to the fact that protonation of cytosine is necessary to form C^+·GC base triplet under acidic pH environment, which is the basement of triplex DNA.[29, 30] To obtain high sensitivity of the assay, a pH of 6.0 was selected in the following experiments.

Given that the Hoogsteen hydrogen bonds of triplex structure is weak, high temperature had adverse effect on the formation of triplex DNA, so the temperature can affect the performance of the sensing system. As shown in Fig. 2B, the ΔAD of the sensing system slightly changed at relatively low temperature, while the value of ΔAD obviously changed when the temperature is above 37 °C. It indicates that the relatively low temperature contributes to the formation of triplex and the aggregation of gold nanoparticles. The maximized ΔAD was obtained at 25 °C. Therefore, 25 °C was selected for further analytical applications.

As spermine can stabilize the triplex structure,[31] the concentration of spermine is a key factor to influence the sensing process. Fig. 2C illustrates how the AD change is related to the concentration of spermine, the highest ΔAD for the assay was obtained when the concentration of spermine was 250 μM. Therefore, 250 μM spermine was employed for the subsequent experiments. We also investigated the influence of the aggregation time on the AD of the sensing system. Fig. 2D shows the maximized ΔAD was reached when the aggregation time was longer than 8 h. Thus, in order to achieve the highest sensitivity, 8 h of aggregation time was selected for the rest of the experiments.

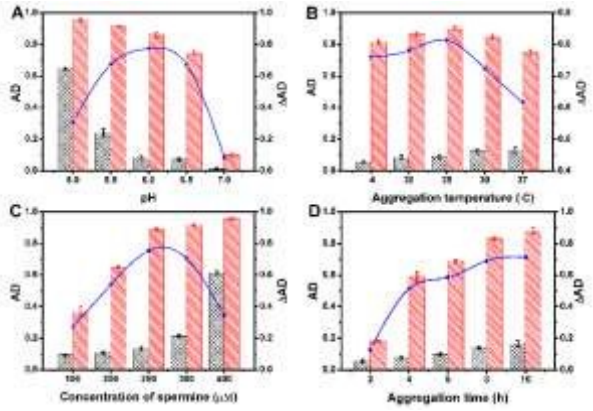

View Article Online
DOI: 10.1039/C6NR09086E

Fig. 2 (A) Effect of the pH value on the performance of the sensing system. (B) Effect of the temperature on the aggregation of gold nanoparticles. (C) Effect of the concentration of spermine on the colorimetric response. (D) Effect of the aggregation time on the response of the sensing system. Black columns: control experiments; red columns: with 5.0 nM of target DNA. Blue lines represent the ΔAD at different conditions. The concentrations of HP, H1 and H2 were 5.0 nM, 100 nM and 100 nM. The error bars indicate the standard deviations of three replicates.

Detection of DNA

To demonstrate the applicability of this colorimetric sensing strategy, different concentrations of target DNA were tested under optimal experimental conditions. As shown in Fig. 3A, with the increased concentration of target DNA, the color of the AuNPs solution was gradually changed from red to blue. Meanwhile, the UV-vis spectra in Fig. 3B presented that with the increasing of target DNA concentration, the absorbance at 522 nm gradually shifted and decreased. Accordingly, the AD was employed to quantitatively scale the target DNA concentration. A good linear correlation between the AD and the DNA concentration ranging from 10 pM to 0.50 nM was obtained (Fig. C), and a detection limit of 5 pM (S/N = 3) was achieved, which was about 2 orders of magnitude lower than the previously reported AuNPs-based colorimetric DNA assay without signal amplification.[32] This high sensitivity could be primarily attributed to the signal amplification of hybridization chain reaction and the assembly of gold nanoparticles with the triplex formatiom.

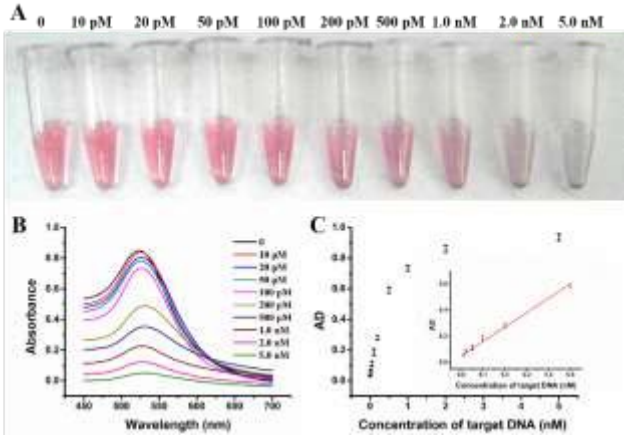

Fig. 3 (A) Photographs showing colorimetric responses of the sensing system in the presence of various concentrations of target. (B) Their corresponding UV-vis absorbance spectra. (C) Plots of aggregation degree (AD) versus the concentration of target DNA. Inset shows the calibration curve for concentrations ranging from 10 pM to 0.50 nM. The error bars indicate the standard deviations of three replicates.

Detection of microRNA

MicroRNAs (miRNAs) are a class of small and noncoding RNAs with approximately 22 nucleotides that participate in gene expression.[33, 34] Recently, much evidence indicates that the development and progression of many types of cancers or diseases is closely related to the aberrant expression of certain miRNAs.[35] Thus, the sensitive detection of cancer-associated miRNAs is of great importance for biological studies and clinical diagnosis. [36] To demonstrate the applicability of the proposed strategy for sensitive detection of miRNA, let-7a was chosen as a proof-of-concept target. As shown in Fig. 4B, the absorbance at 522 nm gradually shifted and decreased with the increased concentration of let-7a. It was found that the AD increased linearly with the concentration of let-7a in the range of 20 pM-0.50 nM with a limit of detection around 10 pM (Fig. 4C), comparable to previously reported methods.[37] Moreover, the specificity of the sensing system was further investigated by adding several let-7 miRNA family members. As shown in Fig. 4E, only in the presence of let-7a, high AD value was obtained, and the AD value of other let-7 miRNAs were comparable to the background signal. This result demonstrated that the one-base difference could be directly discriminated among the miRNA targets, indicating the high specificity of this assay.

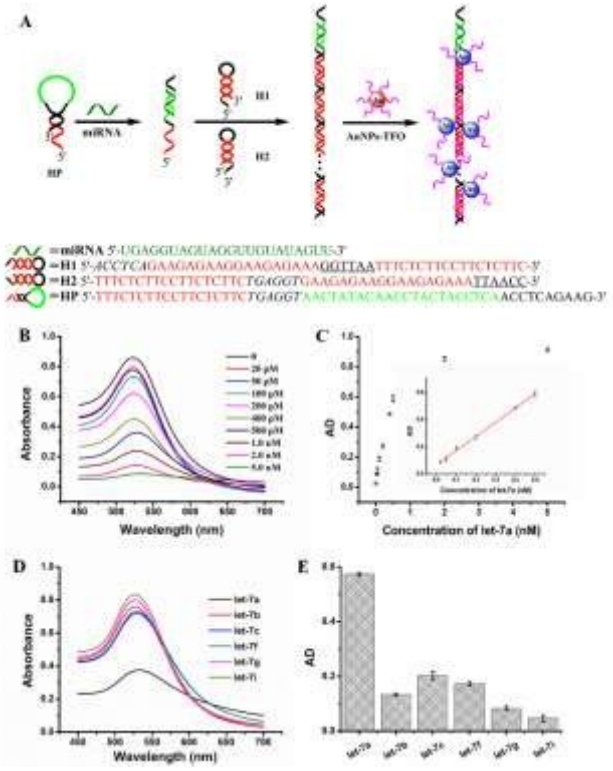

Fig. 4 (A) Schematic illustration of procedures for let-7a detection. (B) UV-vis absorbance spectra of the sensing system in the presence of various concentrations of let-7a. (C) Plots of aggregation degree (AD) versus the concentration of let-7a. Inset shows the calibration curve for concentrations ranging from 20 pM to 0.50 nM. (D) UV-vis absorbance spectra of the sensing system in the presence of different let-7 miRNAs (0.50 nM). (E) Aggregation degree (AD) of the sensing system in the presence of 0.50 nM let-7a and other let-7 miRNAs. The error bars indicate the standard deviations of three replicates.

Detection of ATP

After illustrating that the colormetric sensing strategy was suitable for nucleic acids assay, we attempted to use it in the detection of small molecules, with adenosine triphosphate (ATP) as a model system. ATP, an important substrate in living substrate, plays a critical role in the regulation of cellular metabolism and supplies energy for daily activities.[38] Yet some diseases such as angiocardiopathy, Parkinson's disease and malignant tumors are related to ATP.[39, 40] Thus, the sensitive

detection of ATP in aqueous solution is of great importance. Fig. 5A displays the results of the proposed assay upon detection of different concentration of ATP, we found that the absorbance at 522 nm gradually decreased along with the increasing of the ATP concentration. As shown in the inset of Fig. 5B, a good linear relationship was obtained in the concentration range from 5.0 nM to 0.50 μM, and the detection limit of ATP was estimated to be 5.0 nM, which is lower than those of the previously reported methods.[41, 42] In order to assess the specificity of the sensing system for ATP, the analogs of ATP (GTP, CTP, UTP, dTTP) were added into the reaction system, respectively. Fig. 5C showed the analogs had no obvious interferences on the detection of ATP, which indicated that the proposed strategy exhibited good performance for discriminating ATP against the analogs.

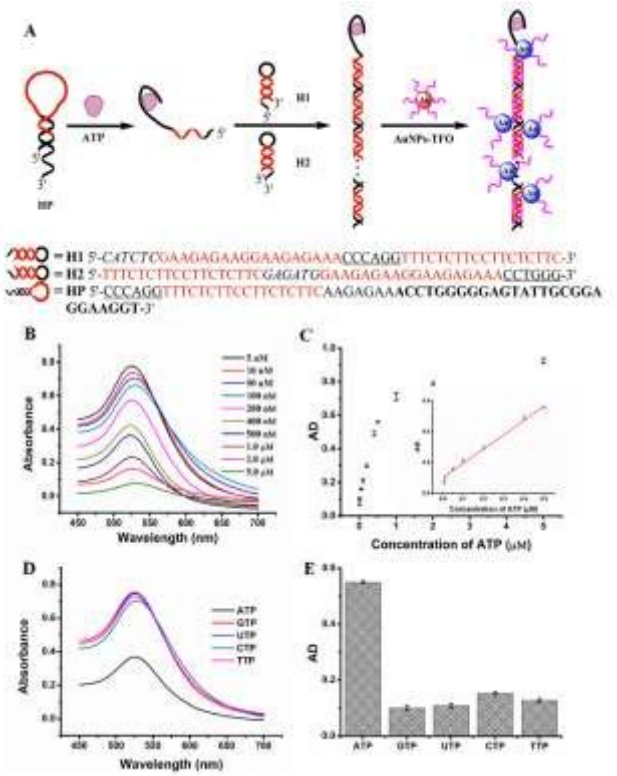

Fig. 5 (A) Schematic illustration of procedures for ATP detection. (B) UV-vis absorbance spectra of the sensing system in the presence of various concentrations of ATP. (C) Plots of aggregation degree (AD) versus the concentration of ATP. Inset shows the calibration curve for concentrations ranging from 5 nM to 0.5 μM. (D) UV-vis absorbance spectra of the sensing system in the presence of ATP, GTP, CTP, UTP and dTTP (0.5 μM). (E) Aggregation degree (AD) of the sensing system in the presence of an equimolar amount ATP and the analogs. The error bars indicate the standard deviations of three measurements.

Detection of PDGF-BB

To complete the demonstration that the platform was universally applicable to a broad range of analyte classes, we investigated whether it could detect protein, using platelet-derived growth factor BB (PDGF-BB) as a model system. PDGF-BB, an important growth factor protein in human platelets, is closely related to tumor cell transformation, tumor growth and progression.[43, 44] Therefore, the methods for highly sensitive and selective detection of PDGF-BB were an urgent and unmet need. As depicted in Fig. 6A, upon increasing additions of PDGF-BB, as expected, the absorbance at 522 nm gradually shifted and decreased. The relationship between the AD and the concentration of PDGF-BB was constructed in Fig. 6B. A good linear correlation was obtained in the concentration range from 20 pM to 1.0 nM. The detection limit for PDGF-BB was estimated to be 20 pM, which compared well with those of the previously reported systems.[45, 46] To investigate the specificity of the proposed strategy for PDGF-BB, we chose five kinds of different proteins as controls: PDGF-AA, PDGF-AB, PDGF-BB, human thrombin and bovine serum albumin (BSA). As shown in Fig. 6C, in the presence of PDGF-AA, PDGF-AB, human thrombin, or BSA (5.0 nM), the AD value had no noticeable changes compared to the background signal, while the AD was greatly increased by the addition of PDGF-BB (1.0 nM), demonstrating that the sensing system had a highly selective response to PDGF-BB.

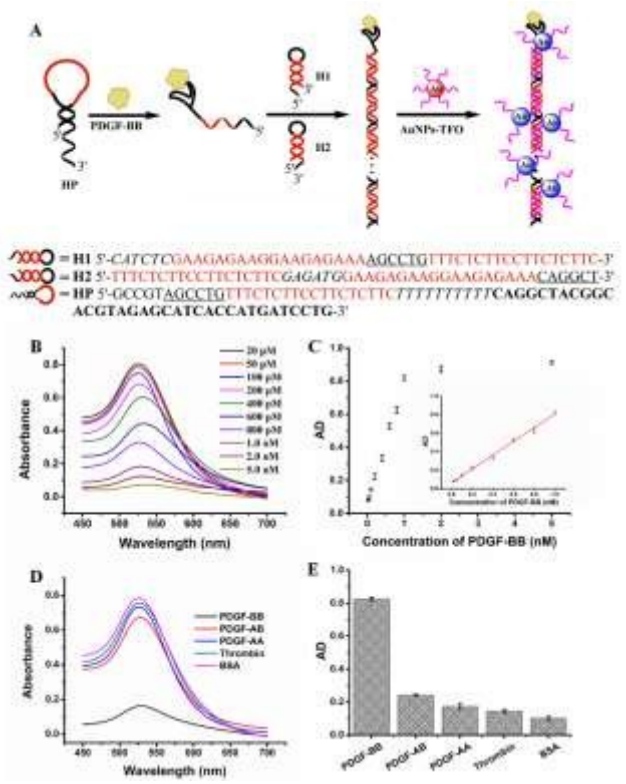

Fig. 6 (A) Schematic illustration of procedures for PDGF-BB detection. (B) UV-vis absorbance spectra of the sensing system in the presence of various concentrations of PDGF-BB. (C) Plots of aggregation degree (AD) versus the concentration of PDGF-BB. Inset shows the calibration curve for concentrations ranging from 20 pM to 1.0 nM. (D) UV-vis absorbance spectra of the sensing system in the presence of PDGF-AA, PDGF-AB, PDGF-BB, human thrombin and BSA, respectively. The concentrations of the above proteins were all 5.0 nM except that PDGF-BB concentration was 1.0 nM. (E) Aggregation degree (AD) of the sensing system in the presence of PDGF-BB and other proteins. The error bars indicate the standard deviations of three measurements.

Conclusions

In summary, we have successfully developed a novel colorimetric sensing strategy for diverse targets assay using

hybridization chain reaction amplification and the assembly of gold nanoparticles through triplex formation. In the absence of targets, the DNA hairpin probes can form rigid triplex structures with TFO-functionalized AuNPs, contributing to the stabilization of dispersed AuNPs and lowering the background signal. By the introduction of targets, the HCR process can be triggered, the dsDNA of HCR products will interact with TFO-functionalized AuNPs to induce the aggregation of AuNPs, resulting in a dramatic absorbance change at 522 nm. The proposed strategy exhibits several advantages: Firstly, the universality of our method is likely to be good, we have demonstrated that it is universally applicable to a broad range of targets, such as nucleic acids, small molecules and proteins. Secondly, the sensitivity of our assay for targets detection is satisfactory due to the negligible background, comparing well with previously reported methods. Thirdly, the sensing system has a highly selective response to targets, thus the assay has great potential to be applied in complex biological media. Finally, the detection can be realized with naked eyes and free of instruments. In addition, this work will likely open the door to joint in-vitro nucleic acid amplification techniques and nanotechnology by triplex formation.

Acknowledgements

This work was supported by the National Natural Science Foundation of China (Grant No. 21375153) and the Natural Science Foundation of Guangdong Province (Grant No. 2016A030310188).

Notes and references

1 F. Xia, X. L. Zuo, R. Q. Yang, Y. Xiao, D. Kang, A. Vallee-Belisle, X. Gong, J. D. Yuen, B. B. Hsu, A. J. Heeger and K. W. Plaxco, Proc. *Natl. Acad. Sci. U S A*, 2010, **107**, 10837-10841.
2 J. Das, K. B. Cederquist, A. A. Zaragoza, P. E. Lee, E. H. Sargent and S. O. Kelley, *Nat. Chem.*, 2012, **4**, 642-648.
3 M. Lin, P. Song, G. Zhou, X. Zuo, A. Aldalbahi, X. Lou, J. Shi and C. Fan, *Nat. Protoc.*, 2016, **11**, 1244-1263.
4 J. Ikbal, G. S. Lim and Z. Gao, *Trends Anal. Chem.*, 2015, **64**, 86-99.
5 R. M. Dirks and N. A. Pierce, *Proc. Natl. Acad. Sci. U S A*, 2004, **101**, 15275-15278.
6 H. M. T. Choi, J. Y. Chang, L. A. Trinh, J. E. Padilla, S. E. Fraser and N. A. Pierce, *Nat. Biotech.*, 2010, **28**, 1208-1212.
7 L. Chen, L. Sha, Y. Qiu, G. Wang, H. Jiang and X. Zhang, *Nanoscale*, 2015, **7**, 3300-3308.
8 X. Yang, Y. Yu and Z. Gao, *ACS Nano*, 2014, **8**, 4902-4907.
9 Z. Wu, G. Q. Liu, X. L. Yang and J. H. Jiang, *J. Am. Chem. Soc.*, 2015, **137**, 6829-6836.
10 W. J. Wang, J. J. Li, K. Rui, P. P. Gai, J. R. Zhang and J. J. Zhu, *Anal. Chem.*, 2015, **87**, 3019-3026.
11 Z. L. Ge, M. H. Lin, P. Wang, H. Pei, J. Yan, J. Y. Shi, Q. Huang, D. N. He, C. H. Fan and X. L. Zuo, *Anal. Chem.*, 2014, **86**, 2124-2130.
12 P. P. Chan and P. M. Glazer, *J. Mol. Med.*, 1997, **75**, 267-282.
13 M. Duca, P. Vekhoff, K. Oussedik, L. Halby and P. B. Arimondo, *Nucleic Acids Res.*, 2008, **36**, 5123-5138.
14 D. Praseuth, A. L. Guieysse and C. Hélène, *Biochim. Biophys. Acta Gene Struct. Expr.*, 1999, **1489**, 181-206.
15 Y. H. Jung, K. B. Lee, Y. G. Kim and I. S. Choi, *Angew. Chem. Int. Ed.*, 2006, **45**, 5960-5963.
16 X. M. Miao, X. T. Guo, Z. Y. Xiao and L. S. Ling, *Biosens. Bioelectron.*, 2014, **59**, 54-57.
17 Z. Zhang, Y. Wang, N. Zhang and S. Zhang, *Chem. Sci.*, 2016, **7**, 4184-4189.
18 Z. Y. Xiao, X. T. Guo and L. S. Ling, *Chem. Commun.*, 2013, **49**, 3573-3575.
19 J. Zheng, J. S. Li, Y. Jiang, J. Y. Jin, K. M. Wang, R. H. Yang and W. H. Tan, *Anal. Chem.*, 2011, **83**, 6586-6592.
20 A. Idili, A. Vallee-Belisle and F. Ricci, *J. Am. Chem. Soc.*, 2014, **136**, 5836-5839.
21 Y. Du, S. Guo, S. Dong and E. Wang, *Biomaterials*, 2011, **32**, 8584-8592.
22 P. Liu, X. H. Yang, S. Sun, Q. Wang, K. M. Wang, J. Huang, J. B. Liu and L. L. He, *Anal. Chem.*, 2013, **85**, 7689-7695.
23 Z. B. Li, X. M. Miao, K. Xing, A. H. Zhu and L. S. Ling, *Biosens. Bioelectron.*, 2015, **74**, 687-690.
24 J. Zheng, Y. P. Hu, J. H. Bai, C. Ma, J. S. Li, Y. H. Li, M. L. Shi, W. H. Tan and R. H. Yang, *Anal. Chem.*, 2014, **86**, 2205-2212.
25 S. R. Aragon and R. Pecora, *J. Chem. Phys.*, 1976, **64**, 2395-2404.
26 O. A. Alsager, S. Kumar, G. R. Willmott, K. P. McNatty and J. M. Hodgkiss, *Biosens. Bioelectron.*, 2014, **57**, 262-268.
27 J. H. Chen, J. L. wen, L. Zhuang and S. G. Zhou, *Nanoscale*, 2016, **8**, 9791-9797.
28 L. E. Xodo, G. Manzini and F. Quadrifoglio, *Nucleic Acids Res.*, 1990, **18**, 3557-3564.
29 D. Yao, H. Li, Y. Guo, X. Zhou, S. Xiao and H. Liang, *Chem. Commun.*, 2016, **52**, 7556-7559.
30 T. Li, D. Ackermann, A. M. Hall and M. Famulok, *J. Am. Chem. Soc.*, 2012, **134**, 3508-3516.
31 T. Thomas and T. J. Thomas, *Biochemistry*, 1993, **32**, 14068-14074.
32 W. Zhou, X. Gao, D. Liu and X. Chen, *Chem. Rev.*, 2015, **115**, 10575-10636.
33 K. K. H. Farh, A. Grimson, C. Jan, B. P. Lewis, W. K. Johnston, L. P. Lim, C. B. Burge and D. P. Bartel, *Science*, 2005, **310**, 1817-1821.
34 Y. Zhang and C. Y. Zhang, *Anal. Chem.*, 2012, **84**, 224-231.
35 B. Boyerinas, S.M. Park, A. Hau, A. E. Murmann and M. E. Peter, *Endocr. Relat. Cancer*, 2010, **17**, F19-F36.
36 A. W. Wark, H. J. Lee and R. M. Corn, *Angew. Chem. Int. Ed.*, 2008, **47**, 644-652.
37 R. Tian and X. W. Zheng, *Anal. Sci.*, 2016, **32**, 751-755.
38 D. E. Atkinson and G. M. Walton, *J. Biol. Chem.*, 1967, **242**, 3239-3241.
39 E. H. Abraham, P. Okunieff, S. Scala, P. Vos, M. J. S. Oosterveld, A. Y. Chen, B. Shrivastav and G. Guidotti, *Science*, 1997, **275**, 1324-1326.
40 C. Ma, C. Lin, Y. Wang and X. Chen, *Trends Anal. Chem.*, 2016, **77**, 226-241.
41 J. Wang, L. Wang, X. Liu, Z. Liang, S. Song, W. Li, G. Li and C. Fan, *Adv. Mater.*, 2007, **19**, 3943-3946.
42 Y. Huo, L. Qi, X. J. Lv, T. Lai, J. Zhang and Z. Q. Zhang, *Biosens. Bioelectron.*, 2016, **78**, 315-320.
43 W. Zhao, S. Schafer, J. Choi, Y. J. Yamanaka, M. L. Lombardi, S. Bose, A. L. Carlson, J. A. Phillips, W. Teo, I. A. Droujinine, C. H. Cui, R. K. Jain, J. Lammerding, J. C. Love, C. P. Lin, D. Sarkar, R. Karnik and J. M. Karp, *Nat. Nanotechnol.*, 2011, **6**, 524-531.
44 M. D. Waterfield, G. T. Scrace, N. Whittle, P. Stroobant, A. Johnsson, A. Wasteson, B. Westermark, C. H. Heldin, J. S. Huang and T. F. Deuel, *Nature*, 1983, **304**, 35-39.
45 C. C. Chang, S. C. Wei, T. H. Wu, C. H. Lee and C.W. Lin, *Biosens. Bioelectron.*, 2013, **42**, 119-123.
46 Z. Z. Zhang and C. Y. Zhang, *Anal. Chem.*, 2012, **84**, 1623-1629.

View Article Online
DOI: 10.1039/C6NR09089C